MAGIC: MAp-Guided Ice Classification System[☆]

D. A. Clausi[*,a], A. K. Qin[*,a], M. S. Chowdhury[a], P. Yu[a], P. Maillard[b]

[a] *Systems Design Engineering, University of Waterloo, Waterloo, ON, Canada*
[b] *Universidade Federal de Minas Gerais, Brazil*

Abstract

A MAp-Guided Ice Classification (MAGIC) system is described and demonstrated. MAGIC is designed specifically to read and interpret synthetic aperture radar (SAR) sea ice images using associated ice maps as provided by the Canadian Ice Service (CIS). An ice chart is manually created at CIS based on the corresponding SAR image as well as other ancillary data to provide ice concentrations, types, and floe sizes within enclosed "polygon" regions. MAGIC uses such information as input and then generates a sensor resolution (pixel-based) ice map for each polygon, a product not feasibly produced manually. The primary feature of the current MAGIC v1.0 is its segmentation module, which is evaluated successfully on a number of images. MAGIC is designed to be used not only as a specific tool for sea ice interpretation but also as a general platform for interpreting generic digital imagery using implemented fundamental and advanced algorithms.

Introduction

The automated interpretation of digital imagery is a complex, challenging task in computer vision. The application of this technology to remote sensing has been an ongoing research endeavor since satellite imagery was first obtained and has become more important with the increased volume of imagery captured by a myriad of satellites. The objective is to automatically apply the following tasks to the digital imagery in order: segment (break image into distinct, uniform regions), cluster (group like regions), and classify (assign class labels to regions).

MAGIC (MAp-Guided Ice Classification) is a software system designed and built to interpret digital imagery. Its primary mandate is to interpret operational SAR (synthetic aperture radar) imagery, but has been implemented to facilitate interpretation of other remote sensing imagery as well as any generic digital imagery. The research represents the amalgamation of many years of published research into a cohesive, usable framework. This was necessitated for two reasons. First, multiple contributors have worked independently to develop algorithms and, as such, there was no means of directly comparing various algorithms on the same platform. Also, without algorithm integration, some domain knowledge was being lost with the natural departure of graduate students and post-doctoral fellows. Second, algorithms were built without any integration with user-friendly visualization tools to properly and efficiently process data and analyze the results. This made it very difficult to run tests and compare results quantitatively and qualitatively. Both of these reasons motivated an operational and research tool that has the potential to be used by other scientists as well, to compare standard and state-of-the-art image interpretation techniques.

MAGIC is an ongoing research endeavor and here version 1.0 is described. MAGIC is unique in that it can interpret SAR sea ice imagery using accompanying operational ice charts. MAGIC uses operator provided polygons in the ice chart as a starting point to interpret ice types on a per pixel basis. This will lead to better comprehension of the ice situation within any particular polygon and provide a more precise estimate of ice type concentrations. MAGIC is not constrained by the ice chart information. For any digital imagery, users can specify the number classes and draw custom polygons, which enables users to independently interpret any part of the image. MAGIC v1.0 is featured with its segmentation module, which utilizes only intensity information as a feature to perform image segmentation. Its validity has been evaluated on many SAR and generic images.

Background

Sea ice monitoring and mapping are among the major operational applications of remote sensing technologies (Carsey, 1989). Sea ice affects operational and environmental activities including ship navigation, marine resource exploitation, and global climate monitoring. Timely and reliable sea ice information is important to facilitate these activities. SAR, as an active satellite microwave sensor, images extensive ice-infested ocean regions both day and night under all weather conditions (Hall, 1998).

SAR sea ice image segmentation is a challenging task due to the large variation of backscatter affected by environmental factors and sensor artefacts. The same ice type can have distinct appearances and different ice types can have similar appearances with respect to different locations, seasons, or varying incident angles.

[☆]Submitted for publication in the Canadian Journal of Remote Sensing/Journal canadien de télédétection. D. Clausi, A. K. Qin, M. Chowdhury, Peter Yu, and P. Malliard. MAGIC: MAp- Guided Ice Classification System. Canadian Journal of Remote Sensing, 36, Suppl. 1, Special Issue: International Polar Year, S13 - S25, 2010.

[*]Corresponding authors (Email: dclausi "at" uwaterloo.ca (D. A. Clausi); kqin "at" uwaterloo.ca (A. K. Qin). Tel. +1 (519) 888-4567 x32604. Fax: +1 (519) 746-4791.)

Environment Canada's Canadian Ice Service (CIS) personnel generate daily charts for ice-infested regions primarily using SAR imagery received from RADARSAT-1/2 satellites (http://www.asc-csa.gc.ca/eng/satellites/). Ice charts are essentially region-based ice distribution maps in which regions with visually homogeneous ice conditions are manually outlined as "polygons" and described by oval "egg code" symbols that summarize the region's ice characteristics. An egg code contains numerical indices to depict the concentrations, types, and floe sizes of ice types inside a specific region, which adopts the World Meteorological Organization (WMO) standards (http://www.wmo.ch). Fig. 1 shows an egg code example. A sample ice chart of the Gulf of St. Lawerence superimposed with egg codes is illustrated in Fig. 2. A more detailed description can be found at the CIS website (http://iceglaces.ec.gc.ca).

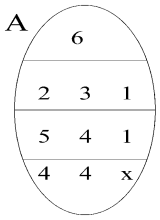

Figure 1: An egg code example. The letter "A" denotes the label of the region. The first row indicates that the total ice concentration is 60%. The second row indicates the individual concentrations for each ice type (thickest to thinnest from left to right). The third row shows a coding for the ice type. The last row indicates the floe size of each ice component ("x" means no/undetermined floe size).

The standardized ice charts only contain regional information. They do not provide at-sensor resolution information about the ice types within each polygon. To perform ice typing for individual pixels is desirable but not manually feasible. Automated methods are preferred for pixel-level interpretation. This is the key motivator for the development of MAGIC.

Other research efforts have been devoted to developing SAR sea ice image interpretation systems. Haverkamp et al. (Haverkamp et al., 1993) introduced a dynamic local thresholding technique for three-category SAR sea ice image classification. Samadani (Samadani, 1995) proposed a finite mixture of Gamma distributions model for estimating proportions of ice classes in a SAR image. Multi-year Ice Mapping System (MIMS) (Fetterer and Ye, 1997) is used for rapid identification of high latitude multi-year ice using a Fisher criterion based local thresholding method. Soh and Tsatsoulis (Soh and Tsatsoulis, 1999) describe an automated SAR sea ice image segmentation system, characterized by dynamic local thresholding, multi-resolution peak detection, and aggregated population equalization spatial clustering. Soh et al. (Soh et al., 2004a) also built a system named Advanced Reasoning using Knowledge for Typing Of Sea Ice (ARKTOS). ARKTOS performs image segmentation using a threshold based watershed merging algorithm, generates a series of attribute descriptors for the segments, and then uses expert rules (Dempster-Shafer theory) drawn from a knowledge database to classify each segment. Karvonen (Soh et al., 2004b) developed a SAR sea ice image classification system based on a modified Pulse-Coupled Neural Network (PCNN).

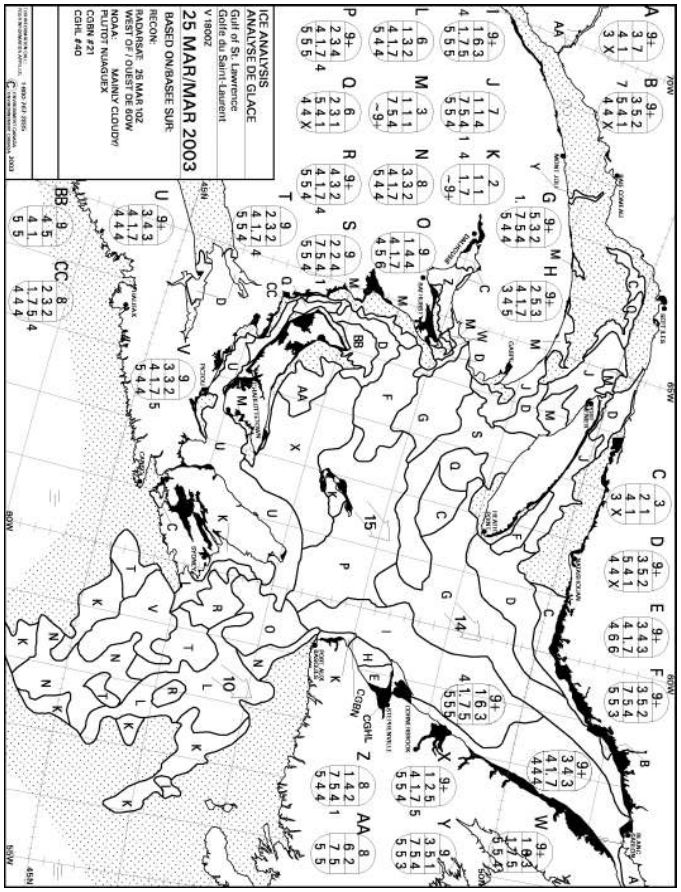

Figure 2: A rotated ice chart example from CIS website (http://iceglaces.ec.gc.ca)

Most of these methods cannot support general sea ice segmentation and classification in the context of various ice types, speckle noise, different seasons and geographical locations of sea fields due to the challenging non-stationary properties of the SAR sea ice imagery.

The basis of this research has been provided by prior publications from the MAGIC research group. Various texture feature extraction approaches applied on SAR sea ice images have been investigated, improved and compared (Clausi and Jernigan, 1998, 2000; Clausi, 2001; Deng and Clausi, 2004a). Novel image segmentation and classification methods have been devised to effectively interpret the SAR sea image imagery (Deng and Clausi, 2005; Yu and Clausi, 2005). A pair of techniques emphasizing the classification task is presented in (Yu and Clausi, 2005) and (Maillard et al., 2005). To have a unified system to encapsulate these algorithms and allow visual assessment of the results is desirable. The MAGIC system has been designed to achieve this goal.

The MAGIC v1.0 System

Overview

MAGIC is built in C++ under the Microsoft .NET 2.0 framework. A schematic representation of the MAGIC v1.0 system architecture is shown in Fig. 3. In MAGIC v1.0, a user-friendly graphical user-interface (GUI) coordinates data input/output (I/O), visualization, and operations. These components are described in this section.

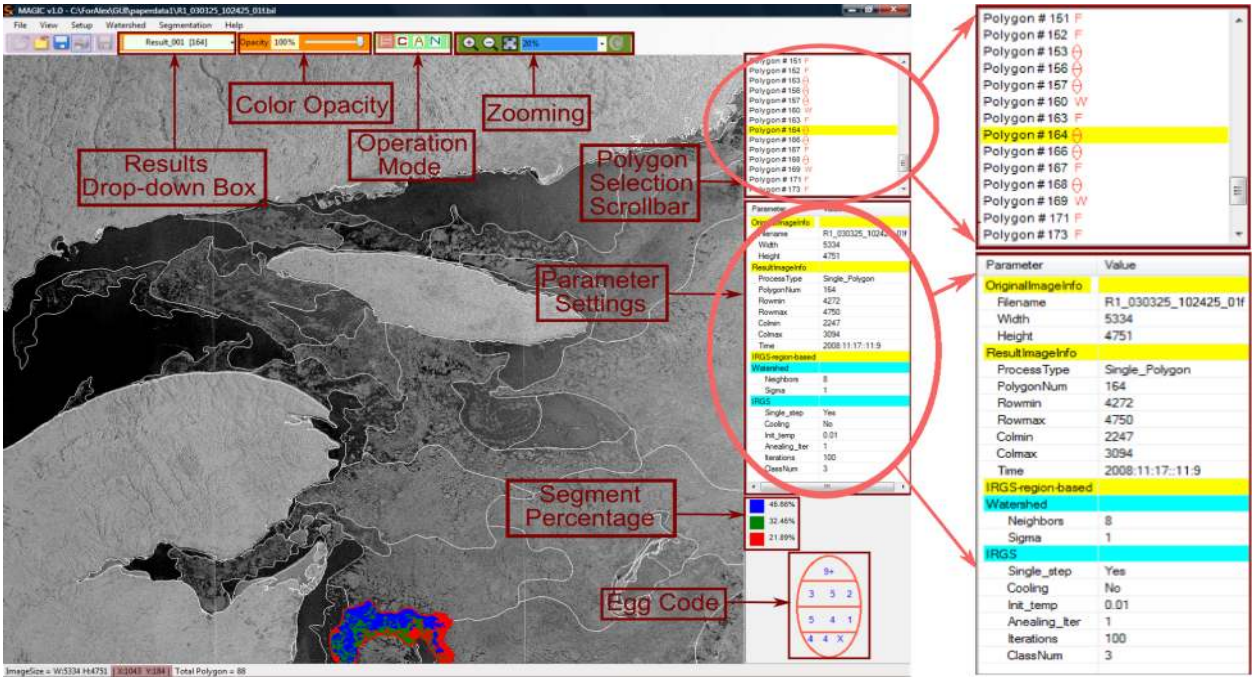

Figure 4: A screen shot of the GUI of MAGIC v1.0.

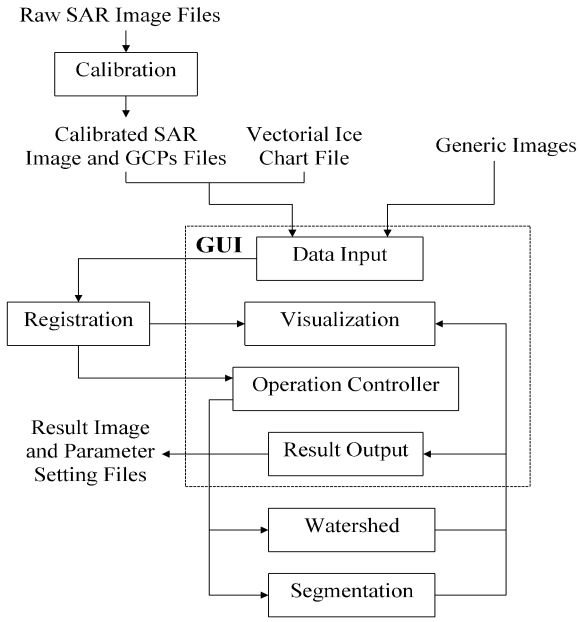

Figure 3: A schematic representation of MAGIC v1.0.

Navigating the GUI

MAGIC's GUI is shown in Fig. 4. The GUI displays all polygons depicted in the ice chart with visible white boundaries that are overlaid on top of the SAR image scene. A listing of the polygons, by polygon number, is found in the Polygon Selection scrollbar at the top right. By clicking a listed polygon, the corresponding polygon region is outlined in red and its associated egg code data is displayed at the bottom right. Correspondingly, by double-clicking within a polygon region, the corresponding polygon in the Polygon Selection scrollbar is highlighted and corresponding egg code is presented. The Zooming tool and mouse can be used to change the image resolution. By clicking, holding, and dragging the mouse, one can pan the image.

Various tasks can be performed by following the menu items: File, View, Setup, Watershed, Segmentation, and Help. Some general information related to the current image such as image directory, image size, coordinate of the current mouse cursor location and the total polygon number in the image is displayed in the title and status bars. In Fig. 4, the SAR image being processed is of size 5334×4751 (pixels) (2×2 block average (Bertoia and Ramsay, 1998) of the original ScanSAR wide image at resolution 100m and pixel spacing 50m) and contains 88 polygons.

Input and Output Files

CIS provides us raw RADARSAT-1 ScanSAR wide mode image files in the .avg format (Bertoia and Ramsay, 1998) along with their accompanying ice chart vector data files in the .txt format. The .avg image files contain SAR sensing parameters, raw image values and GCPs, which cannot be directly used by MAGIC. The ice chart vector data file contains geocoding information for outlines of polygons within the corresponding SAR image scene, as well as egg code information.

A separate calibration program has been build to produce input files for MAGIC from the .avg files. It compensates for varying incident angles and transforms image values into backscattering coefficients. After black image borders being cropped, backscattering coefficients are stored in an .bil file according to the "band-interleaved-by-line" structure. In addition, it extracts GCPs and their associated image Cartesian coordinates from the .avg files and save them in an .txt file. The obtained .bil image file and .txt GCPs file are used together with the ice chart vector data file as input to MAGIC. In fact, MAGIC can also directly take generic bitmap images as input.

Any image segmentation result generated by MAGIC can be saved in the .bil or .bmp format for future viewing. Algo-

rithmic parameter settings related to that result are recorded in an .xml file for future reference.

Data Pre-processing

The CIS ice chart vector data file describes each polygon's profile using a set of latitude/longitude coordinates. To overlay polygons onto the corresponding SAR image scene in the Cartesian coordinate system, registration is required. A Lambert Conformal Conic (LCC) projection (Snyder, 1987) using the Canadian North American datum 1927, followed by a polynomial fitting (Press et al., 1992) with parameters determined via available pairs of the GCP and the image Cartesian coordinate, is applied to convert geographical coordinates of polygon profiles to Cartesian coordinates. Then, a raster mask map is produced in which each registered polygon is filled with its polygon number from the ice chart file. For segmentation, the total number of classes is provided by the egg code information, which equals the number of ice types indicated in the egg code plus open water if total concentration is less then "9+".

Generic digital imagery (remote sensing or otherwise) are read without any ancillary information and the number of classes is set by the user.

Watershed

A watershed (Vincent and Soille, 1991) is a stand-alone algorithm that segments an entire image into regions with closed boundaries. When applied to natural imagery, especially noisy SAR imagery, the watershed algorithm oversegments, which means that the algorithm partitions an image into numerous small regions. The algorithm by Vincent and Soille (Vincent and Soille, 1991) is implemented in MAGIC.

In MAGIC, the over-segmented result is used as an initialization for region-based segmentation, which involves an iterative approach for merging and clustering regions (Yu and Clausi, 2005, 2008). Segmentation techniques using watershed regions instead of individual pixels as the processing unit significantly reduces computational demands.

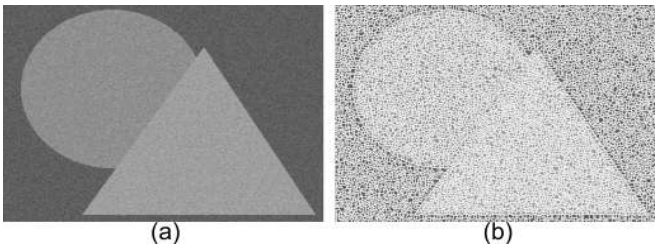

Figure 5: A watershed segmentation example on a synthetic image. (a) A synthetic image (279×378 (pixels)). (b) Watershed segmentation result.

Fig. 5 shows the segmentation result by applying the watershed algorithm on a synthetic image of size 279×378 (pixels). This image is generated by adding Gaussian noise of mean 0 and standard deviation 10 to a clean image composed of three grey levels: 96, 144 and 160. A total number of 10,338 closed regions are generated, separated by white boundaries.

Segmentation Process

The segmentation method is selected via the menu item and popup windows allow for algorithm parameters to be modified. Segmentation can be performed using either individual pixels or regions generated by the watershed algorithm as a starting point. For regions, a region adjacency graph (RAG) structure (Li, 2001) is constructed from the over-segmented watershed regions. Each node in the RAG represents a watershed region and links between nodes denote the common boundaries between neighboring watershed regions. The segmentation approach is then formulated on the RAG instead of the regular image lattice.

MAGIC provides four different operation modes for segmentation processing: (1) Single-polygon mode allows segmentation on a selected polygon created by an ice map. (2) Custom-polygon modes allow segmentation on a single user-drawn polygon. (3) All-polygons mode sequentially segments all polygons created by an ice map in a whole SAR scene. (4) No-polygon mode segments full images, SAR or otherwise.

The algorithm progress is displayed in the status bar located at the bottom of the GUI, as shown in Fig. 4. The segmentation result is displayed in the viewing window where each polygon region displays distinctly colored segments. Color opacity can be adjusted via the Opacity toolbar so that users can effectively evaluate the result and simultaneously view the SAR scene details. Segment percentages and algorithmic parameter settings leading to that segmentation result are shown at the bottom right and can be optionally saved. The Results Drop-Down box is used for viewing previously saved results for that image.

Among the existing image segmentation methods, the MRF (Markov random field) model based segmentation algorithms (Li, 2001; Panjwani and Healey, 1995; Deng and Clausi, 2004b, 2005; Yu and Clausi, 2005, 2008) have shown promising performance for SAR imagery. In the MRF model, the spatial context is taken into account by formulating the local interactions among neighboring pixels. The segmentation module in MAGIC contains the following methods: K-means (Duda et al., 2000), Gaussian mixture model (Duda et al., 2000), constant MLL (multi-level logistical model) (Li, 2001), variable MLL (Deng and Clausi, 2004b, 2005), graduated increased edge penalty (Yu and Clausi, 2008) and iterative region growing with semantics (IRGS) (Yu and Clausi, 2005, 2008). The method that acts as our state-of-the-art approach is IRGS,which combines the attractive features of edge based and region-growing based segmentation methods.

Segmentation Examples

Segmentation tests of single, custom, all, and no polygons using two RADARSAT-1 SAR sea ice images, one RADARSAT-1 SAR wetland image and one synthetic image are presented. The IRGS algorithm is used exclusively for example purposes using only backscatter as a feature. Algorithmic parameters are fixed for all cases ($C_1 = 5$, $C_2 = 0.4$ for β adjustment, and the total number of iterations is set to 100). Since MAGIC v1.0 does not provide automatic ice type labeling, we manually assign an ice type or open water to each segmented region.

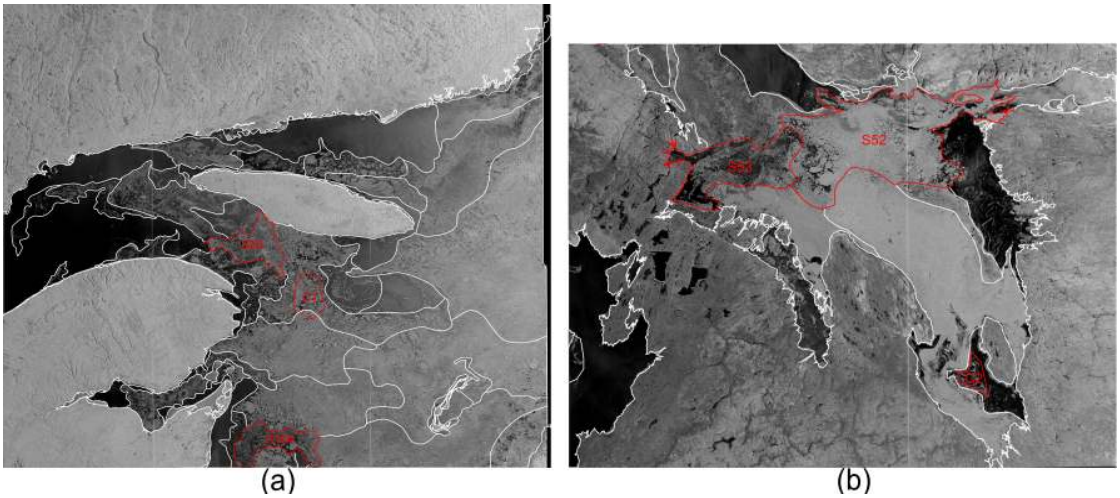

Figure 6: Two operational SAR sea ice images with associated ice chart polygons. (a) SAR image (5334×4751 (pixels) captured on March 25, 2003 over the Gulf of St. Lawrence. S85 and S164 represent two single polygons numbered 85 and 164, respectively. C1 represents a user-defined custom polygon. (b) SAR image (4688×3818 (pixels) captured on October 06, 2004 over the Gulf of Boothia (within the Canadian Arctic). S52 and S53 represent two single polygons numbered 52 and 53, respectively.

Table 1: Comparative analysis of egg code derived ice concentrations with concentrations produced with MAGIC. Two polygons are used for each of two operational SAR images. Colors correspond to segmented regions in associated images. "-" indicates that particular ice type is not present in that polygon.

		Multi-year	Second-year	Grey-white	Grey	New	Open Water
Fig. 7	Egg Code %	-	-	20%	60%	20%	-
	Segmentation %	-	-	44%	45%	11%	-
Fig. 8	Egg Code %	-	-	30%	50%	20%	-
	Segmentation %	-	-	22%	46%	32%	-
Fig. 9	Egg Code %	50%	30%	-	-	10%	10%
	Segmentation %	54%	24%	-	-	10%	12%
Fig. 10	Egg Code %	10%	-	-	40%	30%	20%
	Segmentation %	22%	-	-	37%	9%	32%

Quantitative validation of segmentation results ideally requires corresponding sensor-resolution ground truth. However, provision of sensor-resolution validation field or manually segmented data for SAR sea ice imagery is not feasible. Operationally, classification using WMO standards on a regional basis involves years of experience of sea ice experts and this is the base data that we are utilizing. For the purposes of this research, an arms length senior SAR sea ice expert from CIS carefully analyzed all SAR segmentations presented in this paper and confirmed the accuracy of these segmentations as well as the ice types that were assigned to individual segments. In addition, a test is provided using a synthetic imagery with known ground truth.

Segmentation of Single Polygons

Tests are based on single polygons derived from operational ice maps. Two operational SAR sea ice images with associated ice maps are used. The first image, as shown in Fig. 6(a), was captured on March 25, 2003 over the Gulf of St. Lawrence and has dimension 5334×4751 (pixels). The second image as shown in Fig. 6(b) was captured on October 06, 2004 over the Gulf of Boothia (within the Canadian Arctic) and has dimension 4688×3818 (pixels). Both images are obtained via 2×2 block average (Bertoia and Ramsay, 1998) of the original ScanSAR wide image at resolution 100m and pixel spacing 50m. Two polygons from each scene are tested, namely S85 and S164 highlighted in Fig. 6(a) and S52 and S53 highlighted in Fig. 6(b). Image segmentation results are presented in Figs. 7, 8, 9 and 10. Egg code and segmented ice type concentrations are presented in Table 1.

Fig. 7 shows the segmentation of polygon S85. For this example, three levels of opacity are displayed. Fig. 7(b) shows the segmentation at zero opacity (only boundaries are displayed), Fig. 7(c) shows partial opacity, and Fig.7(d) shows full opacity. This tool easily allows a user to evaluate the quality of the segmentation by varying the opacity to view segmented regions and SAR backscatter simultaneously. The three segmented regions are characterized by darker signatures with about 11% concentration, ice fractures with about 45% concentration and brighter consolidated appearances with about 44% concentration. Since ice floe information provided by the corresponding egg code indicates the same floe sizes for grey white ice and grey ice and no floes for new ice, floe size is not useful for distinguishing grey white ice

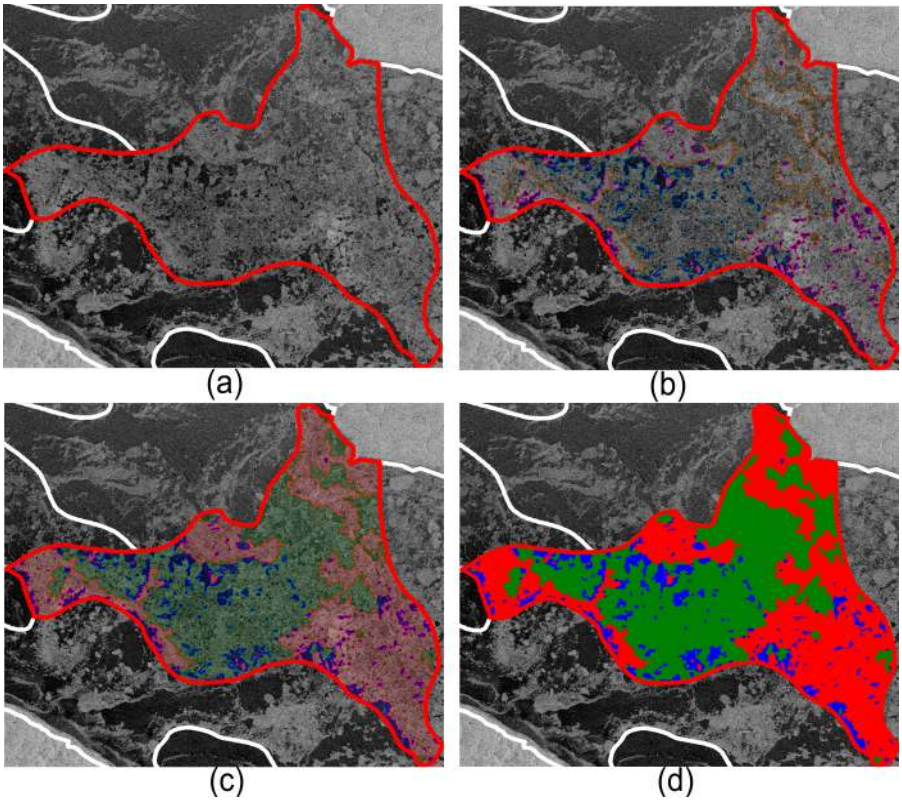

Figure 7: Segmentation result on single polygon S85 in the Gulf of St. Lawrence image. Red regions represent grey-white ice, green regions grey ice and blue regions new ice. (a) Single polygon S85. (b) Segmentation map at zero color opacity. (c) Segmentation map at partial color opacity. (d) Segmentation map at full color opacity.

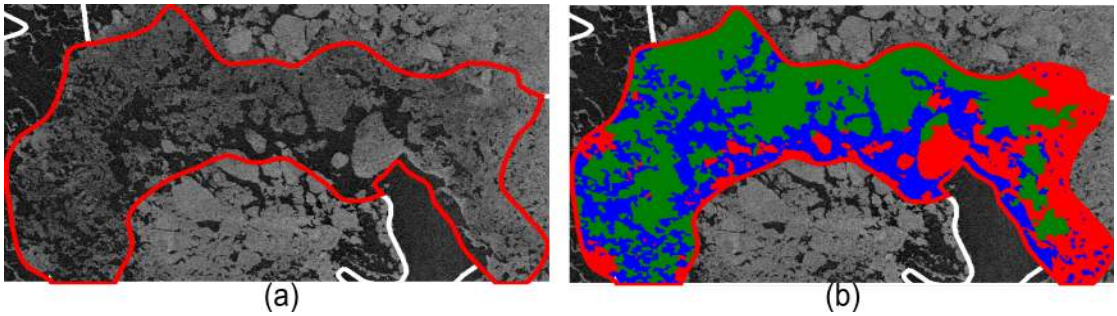

Figure 8: Segmentation result on single polygon S164 in the Gulf of St. Lawrence image. Red regions represent grey-white ice, green regions grey ice and blue regions new ice. (a) Single polygon S164. (b) Segmentation map at full color opacity.

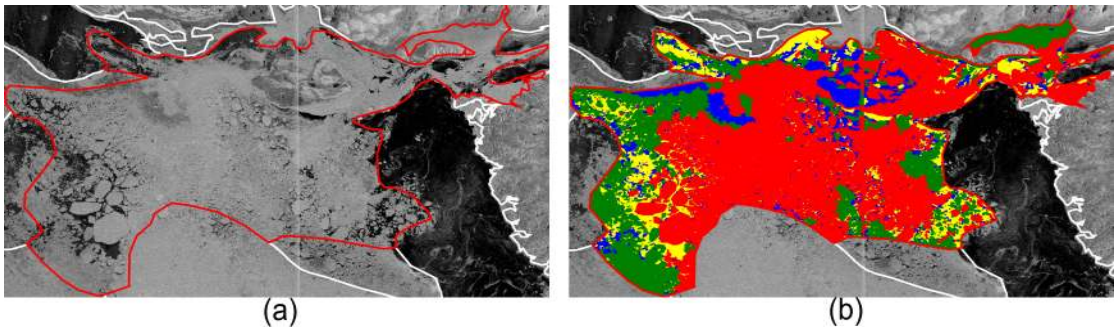

Figure 9: Segmentation result on single polygon S52 in the Gulf of Boothia image. Red regions represent multi-year ice, green regions second-year ice, blue regions new ice and yellow regions open water. (a) Single polygon S52. (b) Segmentation map at full color opacity.

and grey ice. As shown in Table 1, the segmentation results do not match the egg code concentrations.

The three segmented regions with respect to polygon S164 as shown in Fig. 8 have the similar visual properties as those in polygon S85. Table 1 gives the ice labeling result on the segmented regions. Grey ice (46%) is identified with the sim-

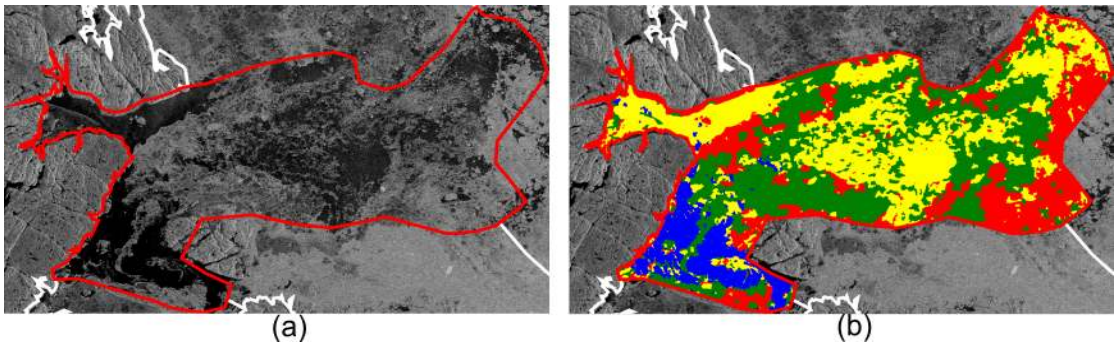

Figure 10: Segmentation result on single polygon S53 in the Gulf of Boothia image. Red regions represent multi-year ice, green regions grey ice, blue regions new ice and yellow regions open water. (a) Single polygon S53. (b) Segmentation map at full color opacity.

ilar concentrations as indicated in the egg code but new ice (32%) has a higher percentage and grey white ice (22%) has a lower percentage.

In the segmentation maps of polygon S52 shown in Fig. 9, the region having bright consolidated appearances with large ice floes is identified as multi-year ice (54%) and the region having relatively darker appearances than the multi-year ice region is identified as second-year ice (24%). Here, the floe size information provided in the associated egg code is used as a clue to visually distinguish multi-year and second-year ice. The region having the darkest appearance is identified as open water (12%) and the region with relatively brighter signatures than the open water region is identified as new ice (10%). Table 1 summarizes this ice labeling result, which resembles the egg code concentrations.

In the segmentation maps of polygon S53 shown Fig. 10, the ice floe information is not useful in the ice type assignment since multi-year ice and grey ice have the same floe sizes while new ice and open water do not contain ice floes. The region containing bright consolidated contents is identified as multi-year ice (22%). Grey ice is assigned to the region having several dark ice fractures (37%). New ice is assigned to the region with the darkest appearance(9%). The region having brighter textures on dark background is identified as the wind-roughened open water(32%). This result is described in Table 1, which does not closely match the egg code concentrations.

For both polygons S52 and S53, total ice concentrations produced with MAGIC are less than those given in egg codes, which indicates a tendency of over-estimation of the total ice concentration in egg codes. It is also worth noting that there is an island (Crown Prince Federik Island) on the top right of polygon S52 which is not described in the CIS vector ice chart. Since MAGIC relies on this ice chart file to perform segmentation it cannot avoid partitioning this island. The similar case happens on polygon S53, in which islands (bottom left) are not included in the ice chart. In addition, the ice chart does not continuously approximate the coast line (top left). Again, MAGIC produces a visually meaningful segmentation result. Segmentation results obtained by MAGIC with inaccurate vector ice chart will inevitably misrepresent ice concentrations.

There are various potential sources of error responsible for the mismatch between ice concentrations obtained in segmentation and those given in egg codes as shown in Table 1. Ice analysts work in a real-time production environment with limited time to visually interpret and label an image. While their ability to type and classify ice is considerable, their ability to accurately and consistently estimate concentration over polygons is subject to human error as per feedbacks from CIS personnel, estimated to be in the range of 10% to 20% (10% in high concentration regimes). In addition, ice analysts may use a variety of ancillary information not present in the SAR scene to make an assessment and this information is not available to the automated segmentation algorithm.

Segmentation of Custom Polygons

In custom polygon mode, the user can draw a closed boundary around any area of interest within the image and then segment that region. Here, a custom polygon C1 is highlighted in Fig. 6(a) with the segmentation result shown in Fig. 11. Three classes are specified and these are characterized by dark signatures representing open water or new ice (17%, shown in blue), grey ice fractures in brighter background (24%, shown in green), and bright more consolidated floes representing thin first year ice or grey white ice (55%, shown in red).

Segmentation of All Polygons

All polygon mode segments each polygon in the scene independently. Fig. 12 displays the segmentation maps for Fig. 6 at full color opacity. Each color inside each polygon denotes a particular ice type for that polygon. The ability to cluster like ice types across all polygons in the scene and assign a common color label to each ice type is not yet included in the MAGIC package. There is no definitive technique to do this, however future MAGIC releases are expected to include such technique. One such labeling technique developed by the group is the cognitive reasoning approach (Maillard et al., 2005) and various methods are under current investigation.

Segmentation Without Polygons

To validate the efficacy of MAGIC v1.0 on segmenting generic images other than sea ice, we use one RADARSAT-1 S2 mode image of a wetland region in Brazil (Fig. 13(a)). This image was acquired in April 2004 with supporting validation data. The region of interest is part of a large wetland area ($\approx$ 3500 hectares) known as "Pandeiros" (15°:40' South, 44°:38' West) considered as having an extreme ecological importance due to its situation in a semiarid savanna region. Due to its

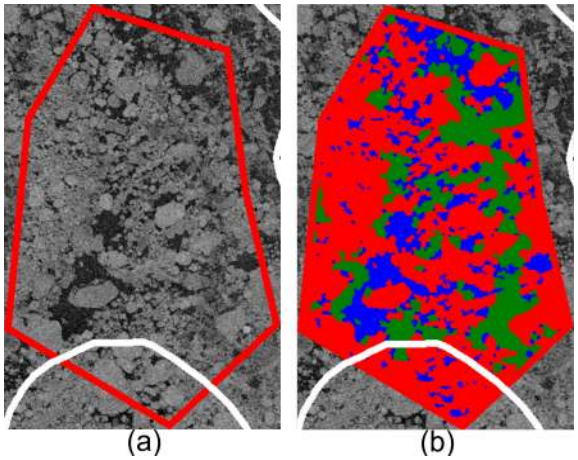

Figure 11: Segmentation result on custom polygon C1 in the Gulf of St. Lawrence image. Red regions represent thin first-year or grey-white ice, green regions grey ice, blue regions new ice or open water. (a) Customized polygon C1. (b) Segmentation map at full color opacity.

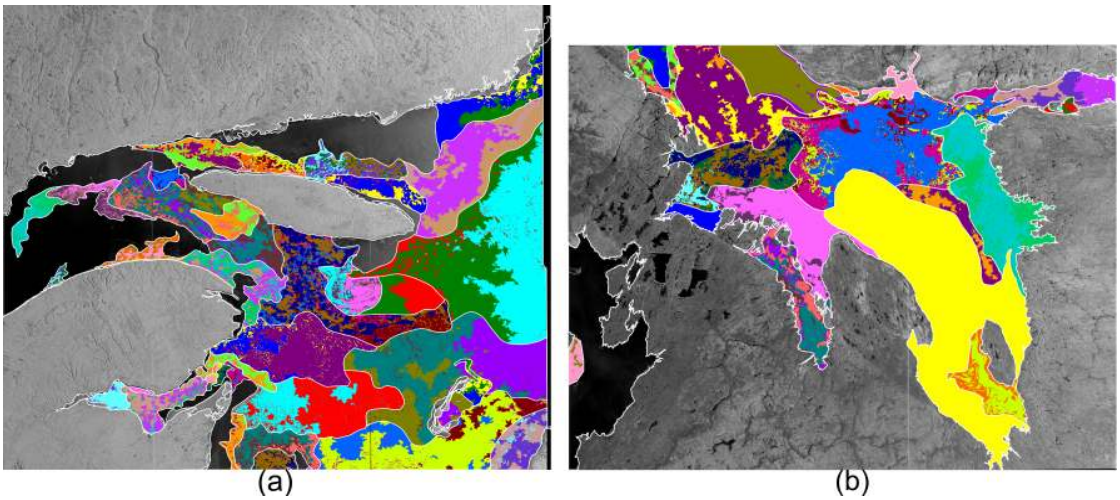

Figure 12: Segmentation result on all polygons of two operational SAR sea ice images. (a) All-polygon segmentation map of the Gulf of St. Lawrence image. (b) All-polygon segmentation map of the Gulf of Boothia image.

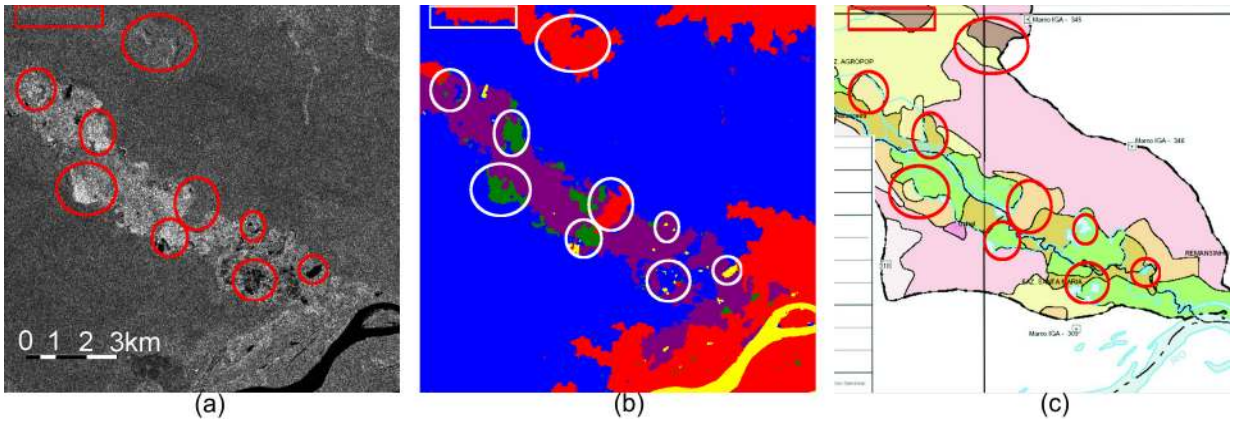

Figure 13: Segmentation result on the "Pandeiros" wetland image with validation map. In the segmentation map, red regions represent high mesophilous forest, blue regions woody savanna and agriculture on dry soils, purple regions shrub wetlands, green regions herbaceous wetlands and yellow regions open water. (a) SAR image (1024×1024 (pixels) at nominal resolution 12.5m) captured in April 2004 over "Pandeiros" wetland. (b) Segmentation map.

short wavelength (C-band) and HH co-polarization configuration, RADARSAT-1 data is not well suited for broad-leaf forest. Conversely, it has shown good potential for mapping flooded vegetation, especially wetlands dominated by herbaceous vegetation (Deng and Clausi, 2001).

Without pre-specified polygons, segmentation is applied to the entire scene with result shown in Fig. 13(b). In this segmentation map, the five colors can be interpreted as follows:

high mesophilous forest are in red (the northern sections represent leaf-on deciduous forests on limestone rock whereas the larger southern part represents riparian forest on fluvial sediments), woody savanna and agriculture on dry soils are in blue, shrub wetlands appear in purple, herbaceous wetlands are in green and open water is in yellow. The main structures as well as a number of small elements (outlined in white) have direct correspondence with those in the validation map (Fig. 13(c)).

The capability of MAGIC to segment generic imagery is also demonstrated using the synthetic image in Fig. 5. The segmentation map shown in Fig. 14 indicates that the three grey levels behind the noise can be well separated as individual regions. The fairly small segmentation error (0.2%) calculated based on the available validation image verifies the segmentation accuracy.

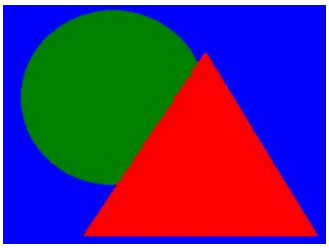

Figure 14: Segmentation result on the synthetic image in Fig. 5.

Table 2 reports the running time of the segmentation algorithm on all of the test images. With larger polygons, there is an exponential increase in computational time due to the increased time and memory involved in storing and using the region adjacency graph (RAG) (Li, 2001). Pixel based segmentation approaches do not require a RAG since the image is stored in a raster format. In the early stages of the IRGS algorithm, there are many regions to consider and this can be very time consuming. Segmentation of all polygons in each scene is completed within an hour, which verifies the operational usage of MAGIC.

Table 2: Running time of segmentation algorithm on test images. Tests were performed on a Windows Vista PC with an AMD 2.3 GHz dual-core CPU using 2 GB memory.

Image Source	Polygon	Segmentation Time (seconds)
The Gulf of St. Lawrence (Fig. 6(a))	S85	23
	S164	25
	C1	8
	All	3250
The Gulf of Boothia (Fig. 6(b))	S52	349
	S53	35
	All	890
"Pandeiros" wetland (Fig. 13(a))	None	823
Synthetic image (Fig. 5(a))	None	35

Future Development

MAGIC v1.0 has demonstrated robust image segmentation for SAR imagery. New features will be incorporated to derive future MAGIC versions. Fig. 15 illustrate the architecture of the future system.

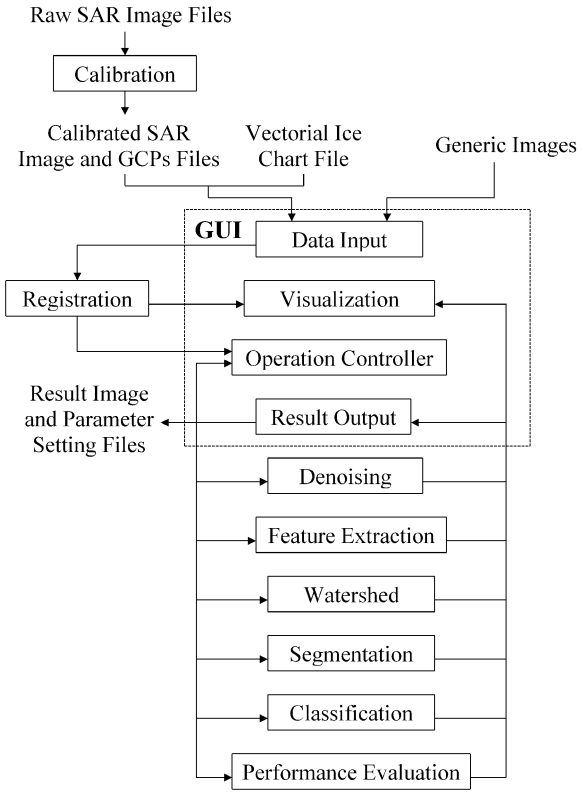

Figure 15: Future MAGIC system architecture.

(1) To reach a broader audience, MAGIC needs to be able to support other remote sensing and generic image formats.

(2) MAGIC v1.0 can only process univariate features. Future MAGIC releases will be multivariate to handle multipolarized SAR data, color images, texture features, and multispectral remote sensing images.

(3) MAGIC will support RADARSAT-2 dual-pol imagery since CIS intends on using both HH and HV bands for operational analysis. The HV band is expected to provide improved open water recognition (Ramsay et al., 2004). The research effort involves the best means to combine these two bands to optimize joint segmentation capability.

(4) MAGIC will incorporate texture extraction methods to augment the backscatter feature. Texture analysis has had a long history in the analysis of SAR sea ice imagery however, its operational use has never been fully realized. Existing routines for co-occurrence, Gabor, and MRF texture feature extraction methods (Clausi and Jernigan, 1998, 2000; Clausi, 2001; Deng and Clausi, 2004a) will be integrated.

(5) MAGIC will incorporate an edge-preserving denoising module (Tomasi and Manduchi, 1998; Yang and Clausi,

2007). Denoising as a preprocessing step for the watershed algorithm that retains edge content will minimize the number of watershed regions generated and, in turn, dramatically reduce the time required for segmentation.

(6) The future MAGIC system will contain linear or nonlinear dimensionality reduction methods (Liu and Motoda, 1998), which can be applied to generate a low-dimensional feature set that retains the important properties of the original image. This is desirable to improve performance and speed of the subsequent operations.

(7) Although application of algorithms to operational imagery is required, for research and development purposes, being able to generate artificial SAR sea ice imagery where the ice class of each pixel is known would be useful (Wong et al., 2009).

(8) MAGIC will incorporate a classification module. Segmented regions can be assigned to a class based on prior information (Yu and Clausi, 2005; Maillard et al., 2005). For SAR sea ice image interpretation, pixel-based ice labeling is the ultimate goal, so including this capability is critical.

(9) In cases where validation data is available, MAGIC will apply a performance evaluation module.

Conclusions

MAGIC is a system designed for the automated interpretation of operational SAR sea ice imagery. In addition, the system has been extended to allow for the interpretation of any generic digital image. MAGIC includes an easy-to-use GUI for segmenting digital images and studying the results. For operational SAR imagery, individual, all, or custom polygon regions can be processed using state-of-the-art and traditional segmentation routines. Future versions of MAGIC will expand and enhance the current functionality, especially with consideration to dual-pol RADARSAT-2 imagery.

Effectively, for SAR sea ice image interpretation, whether polygon, full scene, or sub-scene based, MAGIC will produce a sensor-resolution segmentation, a task not realistically performed by a human. For purposes of environmental monitoring, large regions over multiple dates can be studied for ice type and open water concentrations, improving the local understanding of ice shrinkage in polar regions. For purposes of shipping routes, MAGIC can be used to study local regions and ascertain fairly precise locations of thinner ice that would be preferred for ship navigation. These are important considerations given the world-wide concern of global warming and the costs and risks associated with ships breaking ice unnecessarily.

Aknowledgements

Funding for this project is provided via NSERC Discovery Grant, the Canadian Federal International Polar Year (IPY) project, and GEOIDE (Geomatics for Informed Decisions. http://www.geoide.ulaval.ca/). We specifically thank Dr. Roger De Abreu at CIS for segmentation validation and valuable comments. Thanks is extended to various CIS personnel for support and ongoing data provision.

References

Bertoia, C., and Ramsay, B. 1998. Sea ice analysis and products: cooperative work at the U.S. and Canadian national ice centers. In *the 1998 IEEE International Geoscience and Remote Sensing Symposium (IGARSS'98)*, July 6-10, Seattle, Washington, USA. pp. 1944–1947.

Carsey, F. 1989. Review and status of remote sensing of sea ice. *IEEE Journal of Oceanic Engineering*, Vol. 41, No. 2, pp. 127–138.

Clausi, D.A. 2001. Comparison and fusion of co-occurrence, Gabor, and MRF texture features for classification of SAR sea ice imagery. *Atmosphere and Oceans*, Vol. 39, No. 4, pp. 183–194.

Clausi, D.A., and Jernigan, M.E. 1998. A fast method to determine co-occurrence texture features. *IEEE Transactions on Geosciences and Remote Sensing*, Vol. 36, No. 1, pp. 298–300.

Clausi, D.A., and Jernigan, M.E. 2000. Designing Gabor filters for optimal texture separability. *Pattern Recognition*, Vol. 33, No. 11, pp. 1835–1849.

Deng, H., and Clausi, D.A. 2001. Mapping seasonal flooding in forested wetlands using multi-temporal RADARSAT SAR. *Photogrammetric Engineering and Remote Sensing*, Vol. 67, No. 7, pp. 857–864.

Deng, H., Clausi, D.A. 2004a. Gaussian MRF rotation-invariant features for image classification. *IEEE Transactions on Pattern Analysis and Machine Intelligence*, Vol. 26, No. 7, pp. 951–955.

Deng, H., and Clausi, D.A. 2004b. Unsupervised image segmentation using a simple MRF model with a new implementation scheme. *Pattern Recognition*, Vol. 37, No. 12, pp. 2323–2335.

Deng, H., and Clausi, D.A. 2005. Unsupervised segmentation of synthetic aperture radar sea ice imagery using a novel Markov random field model. *IEEE Transactions Geoscience and Remote Sensing*, Vol. 43, No. 3, pp. 528–538.

Duda, R.O., Hart, P.E., and Stork, D.G. 2000. *Pattern Classification*, 2nd Edition. Wiley-Interscience.

Fetterer, C.B., and Ye, J. 1997. Multi-year ice concentration from radarsat. In *the 1997 IEEE International Geoscience and Remote Sensing Symposium (IGARRS'97)*, August 3-8, Singapore. pp. 402–404.

Hall, D. 1998. Remote sensing of snow and ice using imaging radar. In *Manual of Remote Sensing, Volume 2, Principles and Applications of Imaging Radar*, 3rd Edition. Edited by F.M. Henderson, and A.J. Lewis. Wiley, New York, USA. pp. 677–703.

Haverkamp, D., Soh, L.K., and Tsatsoulis, C. 1993. A dynamic local thresholding technique for sea ice classification. In *the 1993 IEEE International Geoscience and Remote Sensing Symposium (IGARRS'93)*, August 18-21, Tokyo, Japan. pp. 638–640.

Li, S.Z. 2001. *Markov Random Field Modeling in Computer Vision*, 2nd Edition. Springer-Verlag, New York, USA.

Liu, H., and Motoda, H. 1998. *Feature Extraction, Construction and Selection: A Data Mining Perspective*, 1st Edition. Springer.

Maillard, P., Clausi, D.A., and Deng, H. 2005. Map-guided sea ice segmentation and classification using SAR imagery and a MRF segmentation scheme. *IEEE Transactions Geoscience and Remote Sensing*, Vol. 43, No. 12, pp. 2940–2951.

Panjwani, D.K., and Healey, G. 1995. Markov random field models for unsupervised segmentation of textured color images. *IEEE Transactions on Pattern Analysis and Machine Intelligence*, Vol. 17, No. 10, pp. 939–954.

Press, W.H., Flannery, B.P., Teukolsky, S.A., and Vetterling, W.T. 1992. *Numerical Recipes in C: The Art of Scientific Computing*, 2nd Edition. Cambridge University Press, UK.

Ramsay, B., Flett, D., Andersen, H.S., Gill, R., Nghiem, S., and Bertoia, C. 2004. Preparation for the operational use of RADARSAT-2 for ice monitoring. *Canadian Journal of Remote Sensing*, Vol. 30, No. 3, pp. 415–423.

Samadani, R. 1995. A finite mixture algorithm for finding proportions in SAR images. *IEEE Transactions on Image Processing*, Vol. 4, No. 8, pp. 1182–1186.

Snyder, J.P. 1987. *Map Projections - A Working Manual*. United States Government Printing Office, Washington D.C., USA.

Soh, L.K., and Tsatsoulis, C. 1999. Unsupervised segmentation of ERS and radarsat sea ice images using multiresolution peak detection and aggregated population equalization. *International Journal of Remote Sensing*, Vol. 20, No. 15-16, pp. 3087–3109.

Soh, L.K., Tsatsoulis, C., Gineris, D., and Bertoia, C. 2004a. ARKTOS: an intelligent system for SAR sea ice classification. *IEEE Transactions on Geoscience Remote Sensing*, Vol. 42, No. 1, pp. 229–248.

Soh, L.K., Tsatsoulis, C., Gineris, D., and Bertoia, C. 2004b. Baltic sea ice SAR segmentation and classification using modified pulse-coupled neural networks. *IEEE Transactions on Geoscience Remote Sensing*, Vol. 42, No. 7, pp. 1566–1574.

Tomasi, C., and Manduchi, R. 1998. Bilateral filtering for gray and color images. In *the Sixth International Conference on Computer Vision (ICCV'98)*, January 4-7, Bombay, India. Edited by S. Chandran, and U. Desai. Narosa Publishing House, New Delhi, India. pp. 839–846.

Vincent, L., and Soille, P. 1991. Watersheds in digital spaces: an efficient algorithm based on immersion simulations. *IEEE Transactions on Pattern Analysis and Machine Intelligence*, Vol. 13, No. 6, pp. 583–598.

Wong, A., Zhang, W., and Clausi, D.A. 2009. Icesynth: an image synthesis system for sea-ice segmentation evaluation. In *the Fifth Canadian Conference on Computer and Robot Vision (CVR'09)*, May 25-27, Kelona, British Columbia, Canada.

Yang, X.Z., and Clausi, D.A. 2007. SAR sea ice image segmentation based on edge-preserving watersheds. In *the Fourth Annual Canadian Conference on Computer and Robot Vision (CVR'07)*, May 28-30, Montreal, Quebec, Canada. pp. 426–431.

Yu, Q., and Clausi, D.A. 2005. Sar sea-ice image analysis based on iterative region growing using semantics. *IEEE Transactions Geoscience and Remote Sensing*, Vol. 45, No. 12, pp. 3919–3931.

Yu, Q., and Clausi, D.A., 2008. IRGS: image segmentation using edge penalties and region growing. *IEEE Transactions on Pattern Analysis and Machine Intelligence*, Vol. 30, No. 12, pp. 2126–2139.